Direct Observation of Distinct Nucleation and Growth Processes in Electrochemically Deposited ZnO Nanostructures Using in Situ XANES

ARTICLE *in* THE JOURNAL OF PHYSICAL CHEMISTRY C · FEBRUARY 2008

Impact Factor: 4.77 · DOI: 10.1021/jp075775+

3 AUTHORS, INCLUDING:

Benoit Illy
Imperial College London
15 PUBLICATIONS **384** CITATIONS

SEE PROFILE

Direct Observation of Distinct Nucleation and Growth Processes in Electrochemically Deposited ZnO Nanostructures Using in Situ XANES

Bridget Ingham,[†,‡] Benoit N. Illy,[§] and Mary P. Ryan*[,§]

Industrial Research Limited, P.O. Box 31-310, Lower Hutt, New Zealand, Stanford Synchrotron Radiation Laboratory, 2575 Sand Hill Road, Menlo Park, California 94025, and Department of Materials and London Centre for Nanotechnology, Imperial College London, Exhibition Road, London SW7 2AZ, United Kingdom

Received: July 23, 2007; In Final Form: September 23, 2007

In situ synchrotron X-ray absorption was used to study the nucleation and growth of ZnO nanostructures electrochemically deposited from aqueous solutions. A fixed-energy approach was used, which facilitates faster time resolution for systems that are not amenable to transmission measurements and where species-specific information has so far been elusive. Films formed at low potentials (−0.97 V vs Ag/AgCl) show instantaneous nucleation, continued growth, and coalescence of the nanorods. The resultant film is dense with narrow dispersion of rod diameters. At less negative deposition potentials (−0.77 V vs Ag/AgCl), the nucleation is more protracted, resulting in a polydispersed film. In this higher potential region, the growth rates are slower, and there is less evidence of coalescence in the deposited structures, with continued growth along the *c*-axis only.

Introduction

ZnO nanostructures have great promise in a wide range of applications such as sensors,[1,2] optoelectronic devices,[3,4] piezoelectronic devices,[5] and in cancer treatment and skin protection.[6] Preparation of oxide films by electrodeposition from aqueous solution presents several advantages over other, usually vacuum-based high-temperature techniques: for example, the rate and morphology of the structures can in principle be controlled through several well-defined parameters (electrode potential, current, temperature, pH, etc.), the fact that electrolytic processing is a well-established technology and readily scalable for production, and that the nonequilibrium nature of the electrochemical interface often gives rise to morphologies and compositions not attainable through other, usually high-temperature, routes. The formation of nanostructured ZnO by electrochemical deposition from a simple nitrate solution was first shown by Peulon and Lincot[7] and subsequently by several other groups for a variety of substrates.[8−10] The critical parameters for the formation of nanorods is critically dependent on the applied potential, the concentration of Zn ions, and the solution temperature.[11] However, the mechanism of nanostructured ZnO nucleation and growth under electrochemical conditions is not well-understood and is a key factor for the control of the morphology and therefore the properties of the films.[12]

In the electrodeposition process, as soon as the cathodic potential is applied, a current is generated via the reduction of dissolved oxygen and nitrate ions. Hydroxide ions are produced (see eqs 1 and 2), which increase the local pH in the vicinity of the substrate (cathode) surface and lead to the direct formation of zinc oxide (eq 3). The electrochemical data therefore relate to the reduction reactions (eqs 1 and 2) but the reaction of most interest is the ZnO formation (eq 3).

$$NO_3^- + H_2O + 2e^- \rightarrow NO_2^- + 2OH^- \quad (1)$$

$$\frac{1}{2}O_2 + H_2O + 2e^- \rightarrow 2OH^- \quad (2)$$

$$Zn^{2+} + 2OH^- \rightarrow ZnO + 2H_2O \quad (3)$$

Some information can be inferred from the electrochemical data; however, this is not trivial; for example, electrochemical current efficiencies ranging from 0.1 to 1 (i.e., between 10 and 100%) have been quoted in the literature.[11−14] Some electrochemical quartz crystal microbalance (EQCM) experiments have been performed in attempts to correlate the electrochemical measurements to material deposition,[7,13−15] but these are not species-specific. While growth is observed, it is not possible to correlate this directly with any particular electrochemical process.

Hence, there is a need for real-time, species-specific methods to bridge the gap and allow the film growth to be directly correlated with the electrochemical behavior of the film during deposition. Here, we used synchrotron X-ray absorption spectroscopy during film deposition, while controlling the electrochemistry in situ.

Experimental Procedures

In situ X-ray absorption spectroscopy experiments were conducted on beamline X10C at the National Synchrotron Light Source, Brookhaven National Laboratory. The experimental setup has been described previously.[13] Briefly, the substrate consists of 20 nm Au sputtered onto 6 μm Mylar, which also forms the window of the cell. X-rays penetrate from the reverse side of the window, and the X-ray absorption near-edge spectroscopy (XANES) spectra are collected in fluorescence, while the electrochemistry is controlled inside the cell with a Radiometer Voltalab PGZ402 potentiostat, in conventional three-electrode geometry.

* Corresponding author. E-mail: m.p.ryan@imperial.ac.uk.
† Industrial Research Limited.
‡ Stanford Synchrotron Radiation Laboratory.
§ Imperial College London.

10.1021/jp075775+ CCC: $40.75
Published on Web 02/06/2008

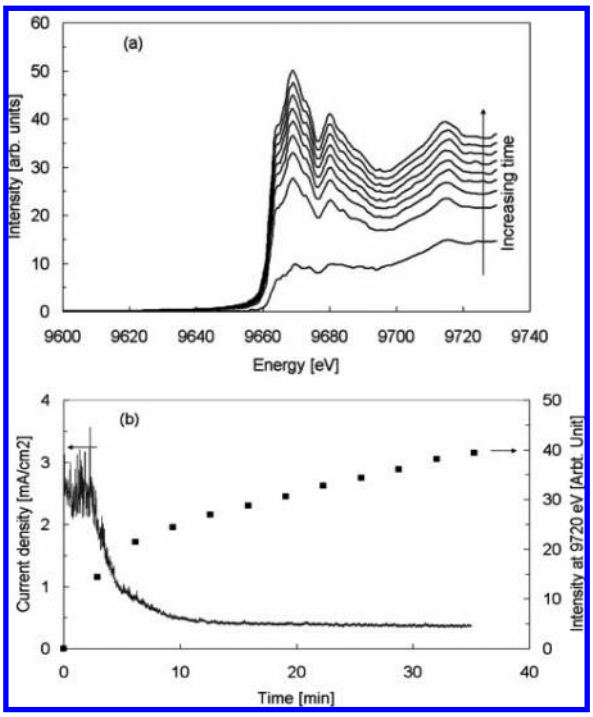

Figure 1. Synchrotron XANES and electrochemical data for a ZnO film deposited from a 5 mM $Zn(NO_3)_2$ solution with 0.1 M KCl electrolyte at −0.97 V vs Ag/AgCl. The temperature of the solution was 70 °C. (a) Repeated scans across the Zn K-edge. (b) Recorded current density during the deposition and value of the X-ray absorption intensity at 9720 eV, as a function of time.

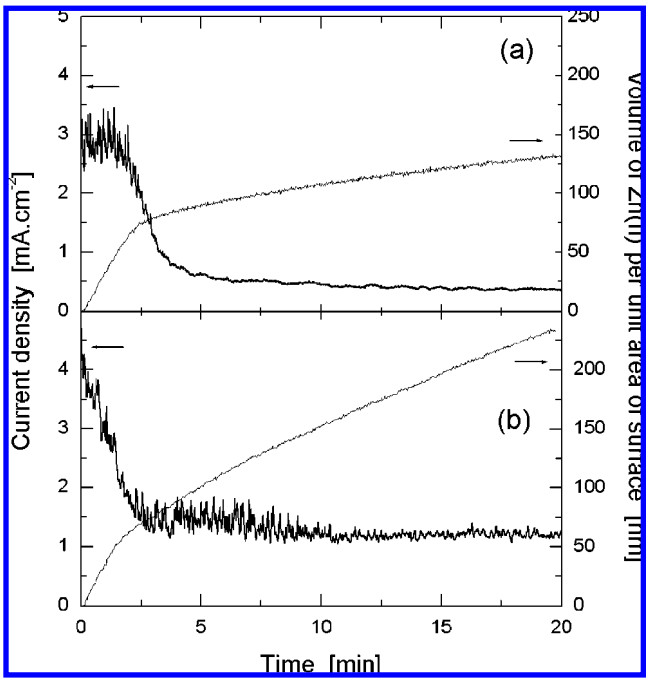

Figure 2. Simultaneous electrochemical current density and film thickness obtained from X-ray absorption intensity at 9725 eV, as a function of time, for ZnO films deposited from a 5 mM $Zn(NO_3)_2$ solution with 0.1 M KCl as the electrolyte at 65 °C. The applied potentials were (a) −0.77 V and (b) −0.97 V vs Ag/AgCl.

$Zn(NO_3)_2$ (Riedel DeHaën, 98%) was dissolved in aqueous solution at a concentration of 5 mM with 0.1 M KCl (BDH, 99%) acting as the supporting electrolyte. The counter electrode was a Pt wire, and the reference electrode was an Ag/AgCl/KCl (3.5 M) reference electrode against which all potentials are quoted (≡ +0.205 V vs NHE). The solution was held at a constant temperature of 65 ± 2 °C throughout the deposition. Complementary microstructural analysis was performed ex situ after collection of the XAS data with scanning electron microscopy using a LEO 1525 field emission microscope (FESEM).

Results

In the past,[17,18] the dissolution of material has been followed in real-time by performing XANES scans with as rapid scan rates as possible (2−3 min). This same technique was initially applied to monitoring the growth of ZnO nanostructures by repeatedly scanning across the XANES region of the Zn K-edge, on a similar time scale. In this setup, the incident X-ray beam penetrates the whole of the sample under investigation, and so the edge height in the XANES region is directly proportional to the amount of material present.

Figure 1a shows a series of XANES scans at the Zn K-edge, taken as ZnO is being deposited from the $Zn(NO_3)_2$ solution. The shape of the curves does not change with time and matches that of bulk ZnO. However, at very short times, when the volume of material being added as a proportion of existing material is very large, two problems arise. First, the spectra are more sensitive to this growth, and consequently, the curves appear to be different. Indeed, if one assumes linear growth and accounts for this in the first scan by dividing by the time, the curves are identical to ZnO.

Second, the nucleation processes, which are thought to dictate the resulting nanostructures, typically occur over a time span of 0−5 min. Therefore, it is not possible to completely capture this process with successive XANES scans. Figure 1b illustrates this: in the time it takes to observe the nucleation peak in the current density, only two XAS data points (corresponding to the edge height) are obtained. To extract sensible growth information for these very short times, one needs to utilize a different approach. Ideally, energy dispersive EXAFS (EDE) would be the tool of choice; however, such measurements cannot be performed in fluorescence geometry, and the deposition process is not amenable to the thin film cell geometry required for transmission measurements.

Rather than repeatedly scanning the energy over the XANES region ($E_0 = -50$ eV to $E_0 = +60$ eV; where here E_0 is the Zn K-edge at 9659 eV), we fixed the energy at a constant value above the edge and measured the signal in a continuous fashion (1 s counting time). This is appropriate since we know that the phase formed is not changing with time and so the shape of the XANES remains the same. The fixed energy chosen for these experiments was 9725 eV. Simultaneously, the deposition current density was also monitored, allowing a direct correlation to be made (Figure 2).

In addition, full XANES scans were taken before the deposition to record the magnitude of the solution signal (which is used as an internal standard, having been calibrated for different concentrations against a ZnO sputtered film of known thickness). Another XANES scan was recorded after the deposition to confirm that the correct phase, ZnO, had been formed. EXAFS spectra were also collected postdeposition for further analysis. In this way, we obtained all the information of the previous method but gained extra information on the nucleation and growth processes in real-time. This is limited only by the time scale required for the measurement of each data point.

Figure 2 presents two examples of the simultaneous deposition and current density curves, obtained at different applied potentials. For the film deposited at −0.77 V (Figure 2a), the

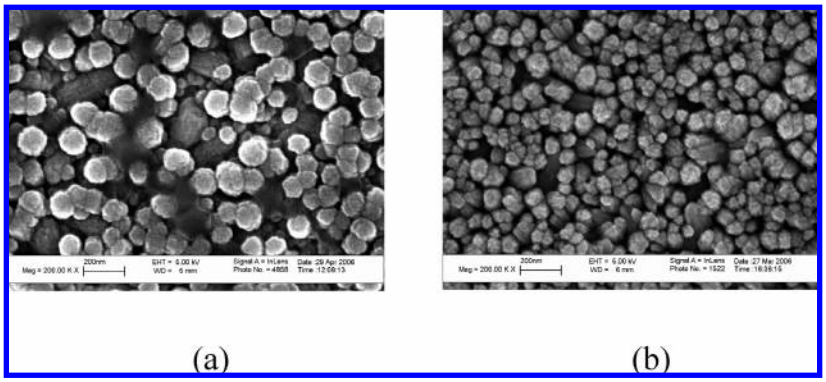

Figure 3. FESEM images of the films in Figure 2, deposited at (a) −0.77 V and (b) −0.97 V for 4 min; scale bar was 200 nm.

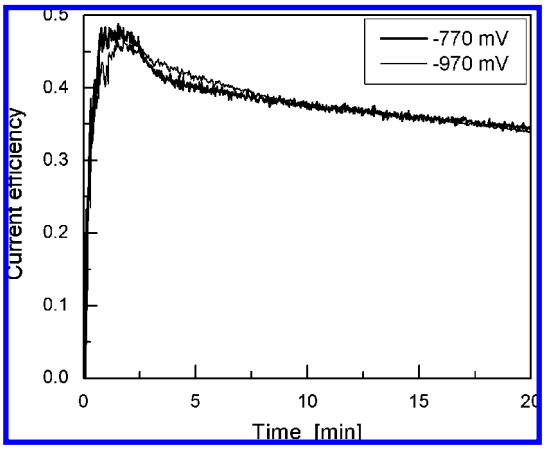

Figure 4. Current efficiencies calculated for the films deposited in Figure 2. $E = -0.77$ V (thick line) and $E = -0.97$ V (thin line).

current density exhibits an initial peak, followed by a decreasing current. In the relative film thickness (expressed here as volume per unit surface area since the nanostructured film is not continuous), two distinct regions of the curve are observed, which one can describe as the nucleation and continuing growth regimes. The film deposited at −0.97 V (Figure 2b) does not demonstrate a peak in the current density; rather, the initial current is high and decays immediately. The distinction between the nucleation and the growth regimes in terms of a change of slope in the growth rate curve is not as pronounced as in the −0.77 V film. The current density after long times is higher than that for the film deposited at −0.77 V, and this is evident in the faster growth of the thickness as a function of time.

Figure 3 shows FESEM images that illustrate the difference in morphology that results when different deposition potentials are used. The film in Figure 3a was deposited at −0.77 V and consists of distinct, well-ordered, hexagonal nanorods 70 nm in diameter. The film in Figure 3b was deposited at −0.97 V, and while the hexagonal motif can still be seen, the rods are less ordered and show signs of coalescence (which becomes more exaggerated with increasing deposition time). It should be noted also that the microscopic analysis and the electrochemical response for samples used in the XAS experiments are consistent with those prepared under normal laboratory conditions.

The current efficiencies are calculated by comparing the amount of material predicted by Faraday's law for the charge passed and the volume of material actually deposited (i.e., is it a measure of how many OH^- ions produced by eqs 1 and 2 result in the formation of ZnO via eq 3). This is shown for the two deposition potentials as a function of time in Figure 4. It is only in the region of the nucleation process ($t < 400$ s) where the two curves deviate to any extent. In the nucleation region, the current efficiencies exhibit a peak that is more pronounced at a less negative potential. This corresponds to the potential that showed a protracted nucleation procedure. At longer times, the efficiency curves are very similar, and there is little to no difference between the two curves obtained for different potentials.

Discussion

Validity of the Method. At energies >50 eV above the absorption edge, the EXAFS oscillations are broader in energy, and their amplitude is damped, as compared to the oscillations at the edge. The selected energy is still close enough to the edge to be sensitive to an increase in signal but not so close as to be drastically affected by changes in the oscillations due to a possible change in local structure. While it is important to note that the positions in energy of the EXAFS oscillations of different phases can vary greatly, the formation of alternative phases (e.g., Zn metal) was not observed in these experiments. Indeed, by performing the successive scanning experiment first, we have shown that the local structure does not change over the time frame of our experiments and that the increase in intensity can only be due to material deposition.

Clearly, the Zn^{2+} in the solution will contribute to the signal; however, in the experimental geometry being used, we are much more sensitive to the signal coming from the nanostructured film grown on the window/electrode. The expected drop in solution signal as a result of decreasing concentration from the Zn species being deposited is negligible. Therefore, a constant value corresponding to the initial solution signal is subtracted from the data. A compact ZnO sputtered film of known thickness was measured in air and with varying concentrations of a Zn^{2+} solution to enable the signal from the solution itself to be used as an internal calibrant.

The self-absorption of the films needs to be considered. At a given energy, the fluorescence signal (I_f) of a film of thickness d, normalized to the incident intensity (I_0), corrected for self-absorption, is[19]

$$I_f/I_0 \propto [1 - \exp(-(\mu_0 + \mu_e)d)]/(\mu_0 + \mu_e) \qquad (4)$$

where μ_0 is the absorption at the incident X-ray energy and μ_e is the absorption at the fluorescent X-ray energy (for Zn Kα1, 8639 eV). Therefore, the film thickness must be corrected by applying

$$d_{actual} = -\ln[1 - (\mu_0 + \mu_e)d_{obsd}]/(\mu_0 + \mu_e) \qquad (5)$$

where $d_{obsd} \propto I_f/I_0$, which holds in the limit of eq 4 for small d values. The function is shown graphically in Figure 5. This

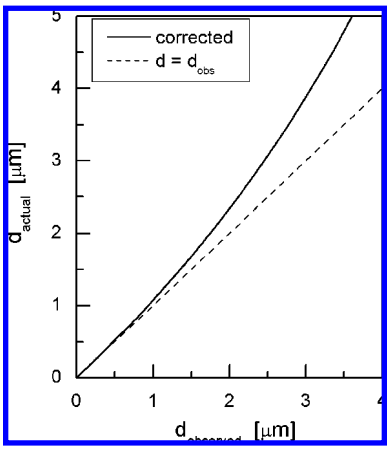

Figure 5. Self-absorption correction function for in situ XAS measurements of ZnO deposition (from eq 5).

corresponds to a difference of 0.7% at 100 nm, 3% at 200 nm, and 6.7% at 1 μm. The curve saturates for $d > 7.6$ μm, meaning that thicknesses greater than 7.6 μm cannot be distinguished. The films produced in our work are typically 200−500 nm thick where these effects are minimal; all data presented here are corrected for self-absorption.

Differences as a Function of Applied Potential. (a) Nucleation and Initial 3-D Growth. As mentioned earlier, the peak in the current density is a characteristic of the nucleation process.[20,21] The nucleation and growth of the first nanostructures result in an increase of the active surface area of the electrode, and thus, the effective current density increases accordingly (where the current density has been calculated based on the planar area of the original Au substrate). The ascending part of the peak is not observed at −0.97 V. Moreover, a comparison of FESEM images obtained for samples where the deposition was halted after the nucleation peak (Figure 3) shows that the nucleation density is lower and the size dispersion is smaller at −0.97 V. These facts strongly indicate that the nucleation process is instantaneous at −0.97 V (or at least faster than the time frame of these experiments <1 s). At the less negative potential of −0.77 V, a continuous nucleation process is observed, and a peak in the current density is evident.

The effective current efficiency increases with time in the nucleation region at both potentials studied, approaching 50% efficiency at the peak of nucleation. This is related to a higher activity of the ZnO electrodeposited surface, for oxygen reduction (e.g., an increase in the oxygen reduction current of ∼40% for a compact electrodeposited ZnO surface vs an Au electrode was measured in this study (not shown)). As ZnO nucleates, the reduction occurs on the more facile surface, and the observed efficiency is seen to increase as more ZnO becomes available for the reaction. As the rods grow and coalesce, the available surface area decreases, so less current is generated, and the apparent efficiency also decreases.

At −0.77 V, the rods grow more slowly than at −0.97 V, and thus, they have a better defined hexagonal shape. However, at −0.77 V, the nucleation is ongoing until the electrode is completely covered, and each nucleation site grows independently until it interacts with the neighboring rods. Therefore, a larger size distribution of rods is observed due to the dispersion of starting times of the growth of each rod. The film grown at −0.97 V has instantaneous nucleation, so the rods have a much narrower dispersion in their starting times and hence in their final size distribution.

(b) Coalescence and 1-D Growth. The sharp change in the slope of the thickness versus time curves observed at both potentials is due to a change in the mode of growth. After the initial nucleation process, the electrode is completely covered with ZnO structures. Growth is then dominated by that perpendicular to the surface of the electrode (i.e., a change from 3-D to 1-D growth), and thus, the deposition rate decreases. This point is reached in shorter times for more negative potentials, where the growth rate in all directions is faster.

This change in slope corresponds to the midpoint of the drop in the current density curves from the initial high value (indicating growth in three directions) to the final constant value (continuous growth of the coalesced film in one direction). This coalescence of the film is not an instantaneous process due to the nonuniform spacing of the rods and, in addition for the film deposited at −0.77 V, the variation in size distribution.

The current efficiency curves exhibit a peak or plateau at the point of coalescence, as the active surface area decreases with the mode of growth changing from 3-D to 1-D. ZnO has a wurtzite structure and exhibits a difference in the polarity of the facets of the rods.[22] From a structural point of view, the main effect of the coalescence is to change the reactive surface of the rods in contact with the solution. Before the coalescence, the lateral surface of the rods increases due to the increase of the height of the rod. As soon as the coalescence begins, the exposed area of the lateral faces of the rods decreases. The fact that the variation of the current efficiency is correlated to the variation of the lateral surface is indicative of the difference in reactivity of the different crystal faces of the rods.

The growth rate observed once the system is in the 1-D regime is lower since no further growth in the direction of the plane can take place. As in the initial growth from the nuclei, the growth at −0.97 V is faster than for −0.77 V, as would be expected due to the larger overpotential for the cathodic reaction.

Conclusion

A modified procedure to collect time-resolved X-ray absorption data has enabled a direct correlation of the growth rate of ZnO nanostructured films to be made with their electrochemical current density as a function of time. Data collected during deposition at −0.77 V evidence distinct nucleation and growth regimes, with a pronounced increase in the current efficiency during the nucleation as compared to later film growth. For a film deposited at −0.97 V, instantaneous nucleation and growth is observed. The low potential film consists of smaller diameter rods with a tight size distribution as compared to films formed at higher potentials.

Certainly, using the repeated scanning method would not have enabled the observation of the distinct change in slope of the thickness versus time obtained for the film deposited at −0.77 V and the less-pronounced change in slope for the film deposited at −0.97 V. This illustrates the power of the fixed energy method for detecting processes in solution that occur on time scales too short to be captured with repeated scans.

Acknowledgment. XAS data reported in this paper were collected at beamline X10C at the National Synchrotron Light Source. Use of the National Synchrotron Light Source, Brookhaven National Laboratory, was supported by the U.S. Department of Energy, Office of Basic Energy Sciences. The authors thank Hugh Isaacs and Kenneth Sutter (Materials Science at BNL) and Larry Fareria and Mike Sansone (NSLS at BNL) for technical support. Funding was provided in part by the New Zealand Foundation for Research, Science and Technology under Contract CO8X0409.

References and Notes

(1) Wan, Q.; Li, Q. H.; Chen, Y. J.; Wang, T. H.; He, X. L.; Li, J. P.; Lin, C. L. *Appl. Phys. Lett.* **2004**, *84*, 3654.

(2) Arnold, M. S.; Avouris, P.; Pan, Z. W.; Wang, Z. L. *J. Phys. Chem. B* **2003**, *107*, 659.

(3) Law, M.; Greene, L. E.; Johnson, J. C.; Saykally R.; Yang, P. D. *Nat. Mater*. **2005**, *4*, 455.

(4) Johnson, J.; Yan, H.; Yang P.; Saykally, R. *J. Phys. Chem. B* **2003**, *107*, 8816.

(5) Kadota, M.; Miura, T. *Jpn. J. Appl. Phys*. **2002**, *4*, 3281.

(6) Willander, M.; Nur, O.; Lozovik, Y. E.; Al-Hilli, S. M.; Chiragwandi, Z.; Hu, Q. H.; Zhao, Q. X.; Klason, P. *J. Microelectron.* **2005**, *36*, 940.

(7) Peulon, S.; Lincot, D. *J. Electrochem. Soc*. **1998**, *145*, 864.

(8) Wong, M. H.; Berenov, A.; Qi, X.; Kappers, M. J.; Barber, Z. H.; Illy, B.; Ryan, M. P.; MacManus-Driscol, J. L. *Nanotechnology* **2003**, *14*, 968.

(9) Illy, B.; Shollock, B. A.; MacManus-Driscoll, J. L.; Ryan, M. P. *Nanotechnology* **2005**, *16*, 320.

(10) Liu, R.; Vertegel, A. A.; Bohannan, E. W.; Switzer, J. A. *Chem. Mater.* **2001**, *13*, 508.

(11) Goux, A.; Pauporte, T.; Chivot, J.; Lincot, D. *Electrochim. Acta* **2005**, *50*, 2239.

(12) Tang, Y.; Luo, L.; Chen, Z.; Jiang, Y.; Li, B.; Jia, Z.; Xu, L. *Electrochem. Commun.* **2007**, in press.

(13) Yoshida, T.; Komatsu, D.; Shimokawa, N.; Minoura, H. *Thin Solid Films* **2004**, *166*, 451.

(14) Pauporte, T.; Lincot, D. *J. Electroanal. Chem.* **2001**, *517*, 54.

(15) Lee, J.; Nam, S. C.; Tak, Y. *Korean J. Chem. Eng.* **2005**, *22*, 161.

(16) Oblonsky, L. J.; Ryan, M. P.; Isaacs, H. S. *J. Electrochem. Soc*. **1998**, *145*, 1922.

(17) Schmuki, P.; Buechler, M.; Virtanen, S.; Isaacs, H. S.; Ryan, M. P.; Boehni, H. *J. Electrochem. Soc.* **1999**, *146*, 2097.

(18) Oblonsky, L. J.; Ryan, M. P. *J. Electrochem. Soc.* **2001**, *148*, 405.

(19) Hooth, C. H.; Bridges, F. *Phys. Scr*. **2005**, *115*, 202.

(20) Southampton Electrochemistry Group, University of Southampton. *Instrumental Methods in Electrochemistry*; Horwood Publishing Limited: Southampton, 2001, Ch. 9.

(21) Canava, B.; Lincot, D. *J. Appl. Electrochem*. **2000**, *30*, 711.

(22) Xu, L.; Guo, Y.; Liao, Q.; Zhang J.; Xu, D. *J. Phys. Chem. B* **2005**, *109*, 13519.